Received March 12, 2020, accepted March 24, 2020, date of publication March 31, 2020, date of current version April 16, 2020.

Digital Object Identifier 10.1109/ACCESS.2020.2984542

A Novel I_C Measurement Without Blanking Time for Short-Circuit Protection of High-Power IPM

ZHAOLIANG MENG[1,2], YUAN YANG[1], YONG GAO[1,2], SHENGSHENG AI[2], ZHENGPENG FANG[2], YANG WEN[1], AND LEI WU[1,3]

[1]Department of Electronic Engineering, Xi'an University of Technology, Xi'an 710048, China
[2]Department of Electrical Engineering, Xi'an Polytechnic University, Xi'an 710048, China
[3]CRRC Xi'an Yongdian Electronic Company Ltd., Xi'an 710016, China

Corresponding author: Yuan Yang (yangyuan@xaut.edu.cn)

This work was supported in part by the National Natural Science Foundation of China under Grant 51477138, in part by the Key Research and Development Program of Shaanxi in Shaanxi, China, under Grant 2017ZDXMGY-130, in part by the College Talent Service Enterprise Engineering under Grant 2017080CG/RC043(XALG009), and in part by the Xi'an Science and Technology Plan Project under Grant 2017074CG/RC037(XAGC009).

ABSTRACT Intelligent power module (IPM) short-circuit protection is a key factor in improving the reliability of power electronics systems. The conventional short-circuit detection method based on monitoring the collector-emitter voltage (V_{CE}) desaturation has a blanking time and is slow to respond to any type of short-circuits. Furthermore, the di_C/dt method cannot be used in the IPM due to the absence of Kelvin emitter. A slow short-circuit protection process can have an irrecoverable and destructive impact on the reliability of the IPM. In this paper, a new high-power IPM topology with an internally integrated shunt is designed to realize real-time current detection, which can achieve fast short-circuit detection without any blanking time. A prototype 1700 V/150 A IPM is manufactured, and a corresponding fast short-circuit protection circuit is designed. Experimental results show the effectiveness of the integrated shunt method as its performance is significantly better than that of the V_{CE} desaturation method. The proposed IPM needs 380 ns and 1.4 μs to detect short-circuits of types I and II, respectively. The short-circuit withstand times for short-circuits of types I and II are 2.06 μs and 0.62 μs, respectively. In addition, the short-circuit energy losses for short-circuits of types I and II are reduced by 66% and 64.3%, respectively, compared to the V_{CE} desaturation method. The proposed method can also be used as a reference for other IPM designs.

INDEX TERMS Blanking time, IPM, IGBT, short-circuit protection, shunt.

I. INTRODUCTION

An intelligent power module (IPM) is a compact and self-regulating module that encapsulates the IGBT chips, diode chips and various driver and protection circuits within the same insulation unit. It is attractive due to its internally integrated logic, control, detection and protection circuits, temperature and current sensors, and other functional modules. In addition, it can send a detection signal to a CPU or DSP for further processing. The volume and weight of IPM are lower compared with those of the IGBT, and its integration, power density and stability are better as well [1], [2].

The short-circuiting of IPM and IGBT modules have been widely investigated in existing research literature. In both these modules, short-circuit detection and protection functions play important roles in the design of driver protection circuit [2]–[5]. These functions include fast detection of the IGBT fault state [3]–[5], limitation of initial peak current [6]–[9], over-current protection [10]–[17] and safe turn-off [18], [19]. In addition, the protection circuits must have noise suppression capabilities in order to prevent fault triggering due to interference [20], [21].

The collector-emitter voltage (V_{CE}) desaturation detection technique is the most commonly used short-circuit protection method [14], [22]–[24]. The desaturation detection technique detects the IGBT turn-on V_{CE}, which is very low under normal conditions. When a short-circuit fault occurs, the IGBT collector current (I_C) will increase to a level that will shift the IGBT operation from the saturated region into the linear region, causing V_{CE} to increase rapidly. The threshold

The associate editor coordinating the review of this manuscript and approving it for publication was Zhehan Yi.

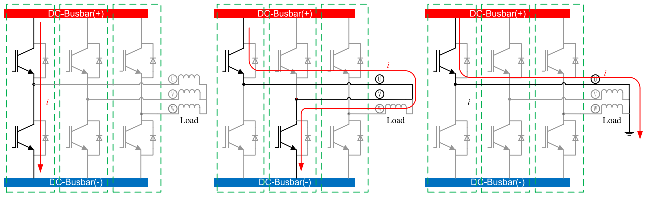

(a) (b) (c)

FIGURE 1. Causes of short-circuit. (a) Bridge arm short-circuit. (b) Load short-circuit. (c) Phase to the ground short-circuit.

voltage levels for desaturation trip can be used to indicate the existence of a short-circuit fault. This is a low-cost simple method based on a simple diode and a comparison circuit, and does not require any current sensor. However, to avoid any incorrect action by the protection circuit during the IGBT turn on, this method generally has a 1-5 μs blanking time. When the IGBT is turned on during the short-circuit state, there will be a large over-current. However, this over-current cannot be detected during this time due to the blanking time, which severely affects the safe use of the IGBT.

In [25], the authors used the de-sat method for protecting a SiC MOSFET from short-circuit failure. The method has a significantly shorter blanking time of 250 ns. However, the operation principles and short-circuit characteristics of SiC MOSFET and Si IGBT are different. Therefore, the value of an acceptable blanking time depends on the specifications of a device and a shorter blanking time for one type of device is not always better than a longer blanking time for another type of device.

To deal with the longer blanking time in the V_{CE} desaturation detection technique, an improved method based on gate voltage detection was proposed in [26]–[29]. During the normal turn-on process of the IGBT, the gate voltage level rapidly increases to Miller platform voltage level. After the charging of the Miller capacitor, the voltage rises to 15 V. On the other hand, if the IGBT is turned on during the short-circuit state, it will not enter the saturation region. Instead, the gate voltage will increase to 15 V at a constant rate without the influence of Miller capacitor. The difference of behavior of the voltage increase between the two aforementioned turn-on processes can be used to detect the short-circuit fault. In the presence of a fault, the relevant protective action can be carried out. This short-circuit detection method can directly and dynamically detect the gate voltage. It is easy to integrate, does not require an isolation circuit, and has a fast response without any detection blanking time. However, the gate voltage is significantly affected by parasitic capacitance and inductance, which requires a complex protection circuit. This circuit is sensitive to noise, highly sensitive to interference, and has low reliability.

Huang proposed a $\mathrm{d}i_C/\mathrm{d}t$ detection method [30], and Wang *et al.* improved it in [15], [31]–[34]. There are two emitters in a packaged IGBT: Kelvin emitter (e) and power emitter (E). The parasitic inductance (L_{eE}) between the two emitters is negligible. The voltage across both ends of L_{eE} reflects the rate of change of I_C, i.e., $\mathrm{d}i_C/\mathrm{d}t$. When the IGBT is in a short-circuit state, I_C and $\mathrm{d}i_C/\mathrm{d}t$ increase rapidly. This behavior can be detected by a relevant circuit, followed by a protective action. The $\mathrm{d}i_C/\mathrm{d}t$ detection method enables dynamic detection with a low cost easy-to-integrate protection circuit. However, the value of L_{eE} is relatively small and difficult to determine exactly, and is strongly affected by the parasitic inductance in the protection circuit. At present, this method is rarely used for IGBT short-circuit protection.

Due to the highly integrated IPM structure, the gate voltage detection method cannot be applied to IPM detection and protection circuits. Similarly, the $\mathrm{d}i_C/\mathrm{d}t$ method cannot be used in the IPM, because there is no e in the IPM and it is impossible to distinguish between E and e. The Mirror current method [35] is also not suitable for the IPM because of its complexity and high cost. Therefore, the protection circuits in IPM modules are mainly based on the V_{CE} desaturation method. This protection method is an indirect detection method, and either has a detection blanking time, or other shortcomings.

Due to the shortcomings of the existing methods, in this paper a low-cost fast current measurement IPM design without blanking time is proposed. The proposed IPM design measures the current by means of shunt resistors of known resistance values connected in series to the IGBT emitter. The current value I_C can be obtained without any blanking time by measuring the voltage across both ends of the shunt resistors. This measurement method is simple, fast, highly accurate and reliable.

The rest of this paper is organized as follows: Section II presents various types of short-circuit conditions, short-circuit failure modes and mechanism analysis, and short-circuit current detection points. The proposed IPM design without a blanking time is presented in Section III, and its detection principle and reliability analysis are shown in Section IV. The fast detection method and protection circuit are discussed in Section V and experimental results are presented in Section VI. The protection performance of the proposed method is analyzed and discussed in Section VII. Finally, the paper is concluded in Section VIII.

II. SHORT-CIRCUIT ANALYSIS

A. SHORT-CIRCUIT TYPES

There are two types of short-circuits: short-circuit I and short-circuit II. Take the three-phase bridge circuit as an example. Short-circuit I refers to the short-circuit in the IGBT bridge arm and is shown in Fig. 1(a). This type of short-circuit

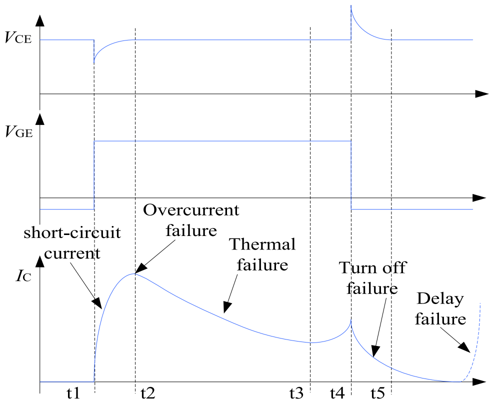

FIGURE 2. IGBT short-circuit characteristic waveforms.

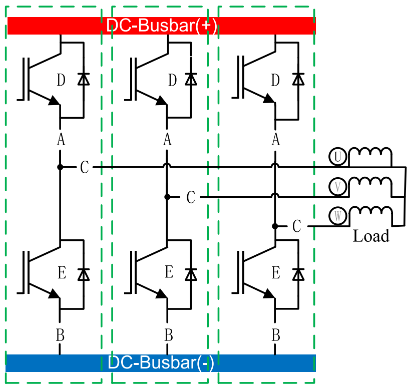

FIGURE 3. Short-circuit current detection points.

is mostly caused by a driver circuit mis-operation or IGBT damage. Short-circuit II refers to the short-circuit between the IGBT bridge arms, usually load short-circuit or phase to the ground short-circuit. It is shown in Figs. 1(b) and 1(c).

When a short-circuit occurs, the high-power IPM must be turned off quickly within the withstand time to avoid any damage, while ensuring that the short-circuit current and voltage during turn-off transition are limited to the short-circuit safe operating area (SCSOA) of the IPM module. In practical applications, detecting and protecting against short-circuit II is more difficult than against short-circuit I.

B. SHORT-CIRCUIT FAILURE MODE AND MECHANISM

An analysis of the short-circuit reveals significant differences between the currents in short-circuit and normal switching processes. In the former process, the current value is in the active region stage and the voltage across both ends of the device is equal to the bus voltage. Therefore, the rated operational current is in the saturation region in the current linearity stage. At this instant, the voltage across both ends of the device is low and consequently the device power consumption is low. As the IGBT current characteristics are dependent on the voltage characteristics, the short-circuit failure mode and its underlying mechanism can be analyzed in detail based on the current waveform in the short-circuit process.

TABLE 1. Short-circuit form corresponding table.

Short-circuit form	Detection point
Bridge arm short-circuit	A, B, D, E
Load short-circuit	A, B, C, D, E
Phase to the ground short-circuit	A, C, D

According to the change of short-circuit current during the short-circuit process, the failure modes can be divided into four types described as follows:

1) Failure due to over-current in the short-circuit during the turn-on transition. The over-current failure mode occurs at the beginning of the short-circuit, represented by t1-t2 in Fig. 2. The short-circuit failure mode is triggered when the instantaneous short-circuit current becomes equal to the latch current.
2) Thermal failure during turn-on transition. The thermal failure mode occurs during short-circuit conduction, where high voltage and large current exist simultaneously, causing a sharp temperature rise of the chip. Thermal failure can take place in the IGBT at various voltage and current levels. The resulting heat generated by high power density causes local hot spots to appear in the silicon wafer. When the critical temperature of the device is exceeded, the failure mode is called intrinsic short-circuit failure mode. The time at which the device reaches the critical temperature is represented by t3 in Fig. 2. The IGBT device should be turned off completely before t3 to avoid any damage.
3) Short-circuit turn-off failure. The turn-off failure mode occurs during the turn-off transition of short-circuit. In this mode, heat accumulation inside the device leads to a high junction temperature, and the depletion zone and carriers are redistributed. During the normal turn-off transition, the device is in the saturation region and the electric field in the drift region is very small. On the other hand, when the device is turned off during a short-circuit, the device is in the active region. Compared with a normal turn-off, the short-circuit turn-off is more likely to cause current wire aggregation, dynamic avalanche and dynamic latch phenomenon, which lead to turn-off failure.
4) Delay failure. Delay failure occurs when the current is not completely reduced to zero after the device is short-circuited and turned off. After a certain time, the device will have a thermal runaway failure because the leakage current and temperature form a positive feedback at high temperatures.

C. SHORT-CIRCUIT CURRENT DETECTION POINT

The objective of short-circuit protection is to accurately identify the short-circuit faults, i.e., to detect the short-circuit

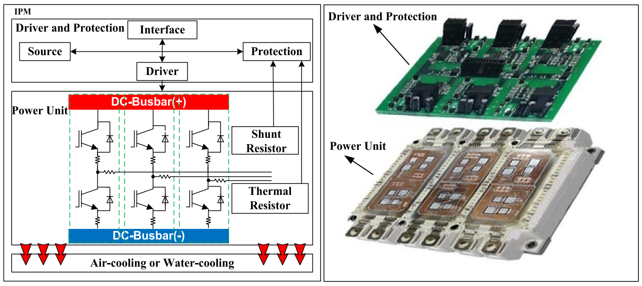

(a) (b)

FIGURE 4. IPM module structure. (a) Block diagram. (b) Physical figure.

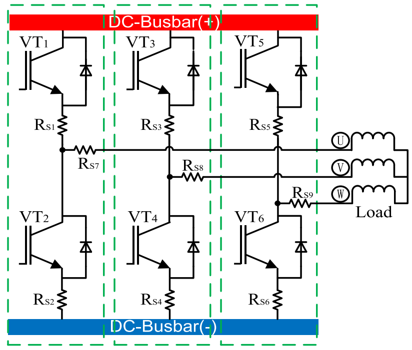

FIGURE 5. Power unit topology.

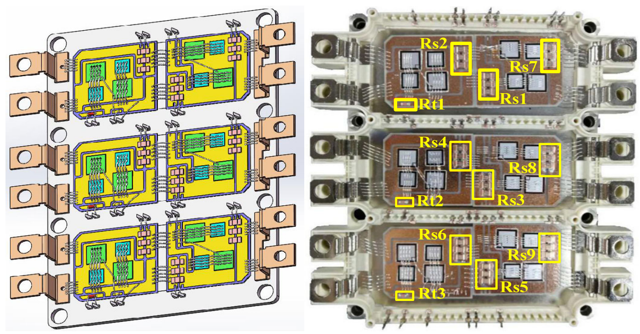

(a) (b)

FIGURE 6. Power Unit. (a) 3D figure of IPM power unit. (b) Physical figure of IPM power unit.

currents. Figure 3 shows the five detection points of the three-phase bridge circuit at which the short-circuit currents can be detected. At each detection point, a specific form of short-circuit can be detected as shown in Table 1.

The detection points A and B can facilitate fast and direct short-circuit protection of the module by leading to the direction of the IGBT emitter current. The detection point C is in series at the three-phase output end, which can directly reflect the current flowing through the IGBT. However, at this point, only the load and phase to ground short-circuits can be detected and the bridge arm short-circuit cannot be detected. The detection points D and E provide short-circuit detection and protection by enabling detection of V_{CE} using the desaturation method, albeit with a certain blanking time. In the next section, a short-circuit detection method for IPM without blanking time is presented.

III. INTELLIGENT POWER MODULE DESIGN WITHOUT BLANKING TIME

A. INTELLIGENT POWER MODULE STRUCTURAL DESIGN

In industry, shunts are commonly used for current detection. With the development of materials, manufacturing and other technologies, the shunts are becoming smaller and smaller around the milliohm level, and the currents and voltages that they can withstand are becoming larger and more accurate. This makes it possible to integrate shunt resistors within a high-power IPM module. We design a 1700 V/150 A IPM module, which integrates the driver and protection circuit, and the power unit. The structure diagram of the module and its physical figure are shown in Figs. 4(a) and 4(b), respectively.

B. TOPOLOGY OF IPM POWER UNIT

The topology diagram of the IPM power unit is shown in Fig. 5, where shunt resistors R_{S1}, R_{S2}, R_{S3}, R_{S4}, R_{S5} and R_{S6} are used to detect bridge arm and load short-circuits, and R_{S7}, R_{S8} and R_{S9} are used to detect load and phase to the ground short-circuits. These shunt resistors can be used to accurately and quickly detect all forms of IPM short-circuit faults, thus enabling fast short-circuit protection. The power unit design of the module and its physical figure are shown in Figs. 6(a) and 6(b), respectively. The shunt resistance parameters are shown in Table 2 . The rated and peak currents of the shunt are 78 A and 390 A, respectively. We design an IPM of 150 A. To fulfill the design requirements, we use three shunts in parallel, e.g., R_{S1} is composed of three shunts in parallel.

Figure 7 shows the switching waveforms of the IPM. As the shunt resistors are very small, the voltages across their both ends can represent the values of I_C flowing through them. In theory, the voltage across a shunt resistor and I_C shown by the purple and green waveforms in Fig. 7, respectively, are linearly correlated. Therefore, the shunt resistors can effectively reflect the change in I_C, irrespective of normal commutation, bridge arm short-circuit, load short-circuit or phase to the ground short-circuit.

IV. DETECTION PRINCIPLE AND RELIABILITY ANALYSIS

The welding of shunt resistors causes parasitic resistance. Therefore, the actual resistance values of the shunt resistors are measured and calibrated via a test circuit shown in Fig. 8. The measured ambient temperature is 25°C. The test current is varied gradually from 10 A to 150 A with a step-size of 10 A. The resistance value of the shunt resistor is measured as 0.34 mΩ.

The shunt generates a certain amount of heat when it is integrated into the IPM. The amount of heat depends on the current ($i_c(t)$) flowing through the shunt resistor and its resistance value (R_{shunt}). The resulting energy loss can be

TABLE 2. Shunt resistance parameters.

Parameters	Values
Power	3 W
Accuracy	1%
Temperature coefficient	<50 ppm/K
Self-inductance	<10 nH
Rated current	78 A
Peak current	390 A
Resistance	1 mΩ

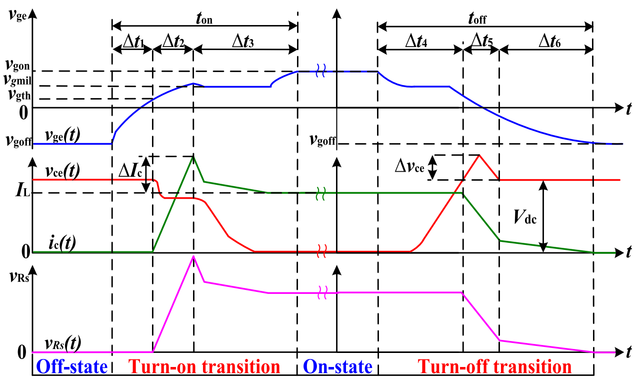

FIGURE 7. Switching waveforms of IPM.

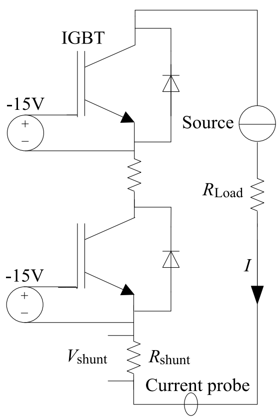

FIGURE 8. Test circuit for measuring the resistance value of shunt resistor.

calculated as follows:

$$E_{loss} = \int_0^t i_c(t)^2 R_{shunt} \, dt \qquad (1)$$

Although the peak value of $i_c(t)$ is very large and the IGBT chip switches constantly, the value of R_{shunt} is equal to 0.34 mΩ, which is very small. When the IPM reaches the

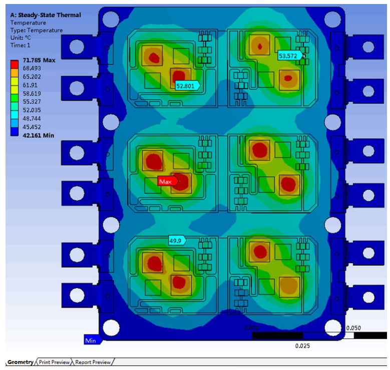

FIGURE 9. Thermal simulation diagram.

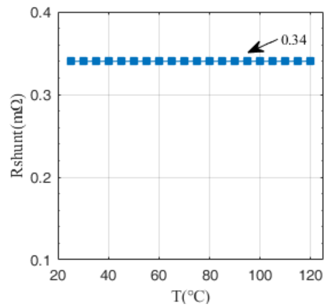

FIGURE 10. Test results of shunt resistance with varying temperature.

thermal steady state, the heat generated by the shunt resistor is negligible compared with the heat generated by the IGBT chips and diodes. To verify this behavior, we use ANSYS to perform thermal simulations shown in Fig. 9. It can be observed from the simulation results that the temperature of the shunt resistor is 20°C lower than that of the IGBT and diode chips, which is consistent with the direct bond copper (DBC) backplane temperature. These results indicate that the heat generated at the shunt resistor has no effect on the interior of the IPM.

The temperature span of IPM can reach hundreds of degrees Celsius from start to thermal stability. In order to ensure measurement accuracy, the shunt resistors cannot have very large temperature coefficients. The data sheets show that the temperature coefficient of a shunt is less than 50 ppm/K at 20°C, which yields an additional deviation of up to 0.5% at 120°C.

A heating test is carried out by placing the IPM module in high and low temperature boxes, so that the temperature is increased from 20°C to 120°C. The test results shown in Fig. 10 confirm that the resistance values of the shunt resistor do not change with an increase in temperature.

V. FAST DETECTION AND PROTECTION CIRCUITS

As mentioned in the previous section, the welding of shunt resistors to the DBC board generates parasitic parameters, especially parasitic inductance. This parasitic inductance is caused by the internal design and external lead wire.

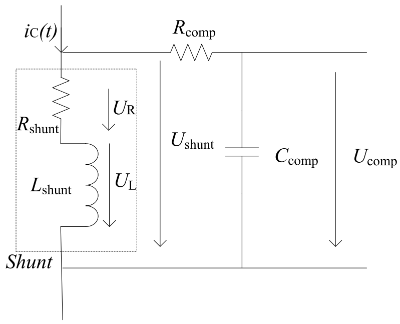

FIGURE 11. Equivalent circuit diagram of shunt resistor.

The equivalent circuit diagram of a shunt resistor shown in Fig. 11 indicates that the total voltage across the shunt resistor (U_{shunt}) includes the resistance and inductance voltages. This voltage can be calculated as follows:

$$U_{\text{shunt}} = R_{\text{shunt}} \cdot i_C(t) + L_{\text{shunt}} \cdot \frac{\mathrm{d}i_C(t)}{\mathrm{d}t} \quad (2)$$

where R_{shunt} and L_{shunt} represent the resistance and parasitic inductance of the shunt resistor, respectively. Equation (2) shows that U_{shunt} depends on L_{shunt} and $\mathrm{d}i_C(t)/\mathrm{d}t$. However, it is difficult to calculate and accurately measure L_{shunt}. Through simulations and experiments, we estimate that L_{shunt} is equal to 0.5 nH.

Based on the parasitic inductance and resistance of the shunt resistor, an RC filter compensation circuit can be used to improve the resistance measurement characteristics. The compensation circuit is shown in Fig. 11, and the relevant calculation to obtain the compensation resistance and capacitance values is as follows:

$$\frac{L_{\text{shunt}}}{R_{\text{shunt}}} = R_{comp} \cdot C_{comp} \quad (3)$$

where R_{comp} and C_{comp} refer to the compensation resistance and capacitance, respectively. As the IPM is a switching device, the switching process influences the internal integrated resistance. Figure 12 shows the simulation results of the behavior of resistance and inductance values versus varying switching frequency. These results are obtained via the ANSYS MAXWELL software. It can be observed that the resistance of the shunt resistor is influenced by the skin effect at higher frequencies [36]. The figure further shows that the resistance of the shunt resistor does not change significantly when the switching frequency is less than 10 kHz, which is significantly higher than the maximum output frequency.

The proposed circuit scheme is shown in Fig. 13. The voltage U_{shunt} ($U_{\text{shunt}} = I_C \cdot R_{\text{shunt}}$) is amplified after passing through the RC filter. The amplified voltage is then input into a comparator circuit where it is compared with a fixed threshold voltage. If it is greater than the threshold, the comparator will output a signal that is the reverse of its input signal. If the input signal is lower than the threshold voltage, the output signal will be the same as the input signal. To ensure the reliability of signal transmission, an optocoupler isolation is used between the power unit and the driver.

TABLE 3. Information of measurement equipment and test bench.

Name	Information
Oscilloscope	Tektronix MDO4104-3, 3 GHz, 5 GS/s
V_{CE}	Pintech N1050B, Probe 1:100,1.5 kV/100 MHz
V_{GE}	Pintech N1050B, Probe 1:50,150 V/100 MHz
I_C	Coaxial shunt, 0.02Ω SSDN-02, 2 kA/800 MHz
L_1	340 μH
L_2	5 μH
L_{loop}	140.5 nH

As the rated current of the IPM is 150 A, we choose the threshold as three times the rated current value, i.e., 450 A. This value corresponds to a threshold voltage of 3.2 V. Therefore, when the amplification of U_{shunt} results in a voltage higher than the threshold voltage, the circuit will commence short-circuit protection.

VI. EXPERIMENTAL RESULTS

In order to evaluate the performance of the proposed short-circuit detection method without blanking time, three types of tests are carried out: double pulse test, short-circuit I test and short-circuit II test. The schematic diagrams of these tests are shown in Fig. 14. In the figure, a film capacitor acts as the DC bus support capacitor. The parasitic inductances are measured in combination with the existing method presented in [31]. The detailed parameters of test bench and measurement equipment used in the test are presented in Table 3 .

A. DOUBLE PULSE TEST

The schematic diagram of double pulse test is shown in Fig. 14(a). This test evaluates whether the shunt resistors affect the normal operation of the module. The test is carried out on both the proposed module and a commercially available 1700 V/150 A module. The bus voltage is increased to 800 V in the experiment. The lower IGBT serves as the device under test and an air-core inductor L_1 serves as the inductive load. The test waveforms are shown in Fig. 15, where the red and blue waveforms correspond to the waveforms obtained from the proposed module and the commercially available module, respectively. From the turn-on and turn-off waveforms shown in Fig.15(a) and 15(b), respectively, it can be observed that the waveforms from the two modules overlap, which indicates that the shunt resistors have no effect on the normal switching of the IPM.

B. SHORT-CIRCUIT I TEST

In order to demonstrate the advantages of the proposed method over the V_{CE} detection method, the proposed IPM is tested with short-circuit I. The schematic diagram of

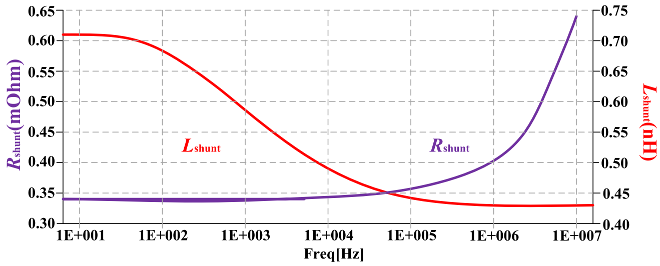

FIGURE 12. Simulated frequency-dependent resistance and inductance of shunt resistor.

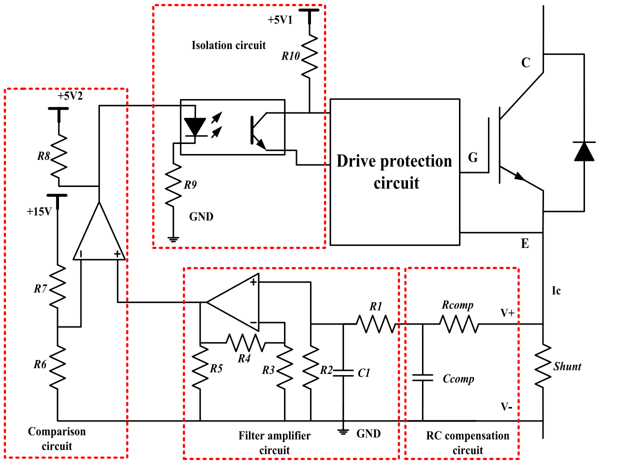

FIGURE 13. Shor-circui detection and protection circuit without blanking tim.

short-circuit I test is shown in Fig. 14(b). The bus voltage is increased to 800 V in the experiment. The lower IGBT serves as the device under test and the upper IGBT is shorted by a thick short copper bar. When a single pulse signal of duration 10 μs is applied to the lower IGBT, the upper and lower bridge arms are directly connected to form short-circuit I.

Figure 16 shows the waveforms of short-circuit I test. The blue and red waveforms represent the waveforms obtained with the V_{CE} desaturation detection method and the proposed detection method, respectively.

It can be seen from the blue waveforms in Fig. 16 that the lower IGBT of IPM starts to turn on at t1. The short-circuit fault occurs at t1, and I_C rises to 1055 A at t4. The short-circuit detection starts at t5. If V_{CE} does not reach the saturated area, the module will be identified as having developed a short-circuit fault, which is followed by a short-circuit protective action. The short-circuit current drops to zero at time t6. The 4.5 μs time duration from t1 to t5 is the blanking time. The short-circuit energy loss is about 3.3 J.

The proposed IPM short-circuit protection threshold is equal to 450 A as mentioned in the previous section. During a normal operation, I_C will not exceed this threshold value. When this threshold is exceeded during a short-circuit, a fault signal will be detected. Therefore, when the red waveform for I_C in Fig. 16 reaches 450 A at t2, the fault signal is detected. It takes 380 ns to detect short-circuit I fault. Due to the circuit delay, the protective action is carried out after 1.3 μs, after which the short-circuit current drops to zero at t4. During this period, the short-circuit peak current is 980 A. It takes about 2.1 μs from the start of fault detection till the end of short-circuit fault, and the short-circuit energy loss is 1.12 J. Comparing the two short-circuit detection methods, it can be concluded that the proposed method has a lower short-circuit loss and a lower fault duration compared with the V_{CE} desaturation detection method.

C. SHORT-CIRCUIT II TEST

In practical applications, short-circuit II is the most difficult to deal with. The schematic diagram of short-circuit II test is shown in Fig. 14(c). The bus voltage is increased to 800 V for this experiment. The lower IGBT serves as the device under test and an air-core inductor L_2 serves as the short-circuit inductor. A short-circuit II will form when a single pulse signal of 10 μs is applied to the lower IGBT.

Figure 17 shows the waveforms of short-circuit II test. The blue and red waveforms correspond to the waveforms of the V_{CE} desaturation detection method and the proposed detection method, respectively. The blue waveform for I_C starts increasing with a positive slope di_C/dt at time t1. The IGBT begins to desaturate at t4. Subsequently, there is no longer any voltage across the inductance and the IGBT enters the short-circuit mode from the saturation mode. After the blanking time, the module will be identified as having a short-circuit fault and at t6, the short-circuit protection starts. According to the experimental data, the short-circuit energy loss is 1.4 J.

When the red waveform for I_C reaches 450 A at t2, the fault signal is detected. The time needed to detect short-circuit II fault is 1.4 μs. Subsequently, the protective action starts and the current drops to zero at t5. The short-circuit energy loss is 0.5 J. Figure 18 shows that the V_{CE} desaturation detection method can detect the fault only after the IGBT desaturation. On the contrary, the proposed method starts the protective action before the IPM enters the short-circuit mode.

VII. ANALYSIS AND DISCUSSION

It can be seen from the experimental data that the proposed detection method does not have any blanking time. In short-circuit I, the V_{CE} desaturation detection method detects and carries out short-circuit protection after a 4.5 μs blanking

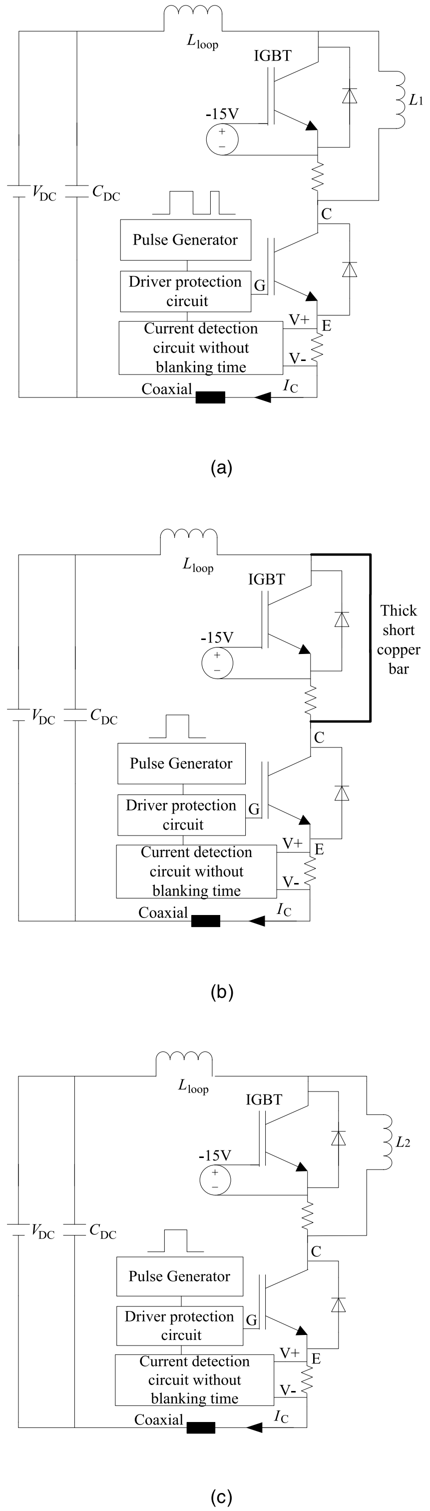

FIGURE 14. **Schematic diagrams of test experiments. (a) Double pulse test circuit diagram. (b) Short-circuit I test circuit diagram. (c) Short-circuit II test circuit diagram.**

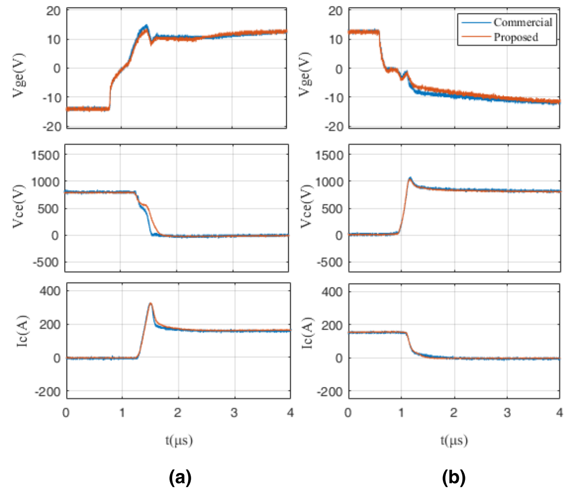

FIGURE 15. **Double pulse test waveforms. (a) Turn-on waveforms. (b) Turn-off waveforms.**

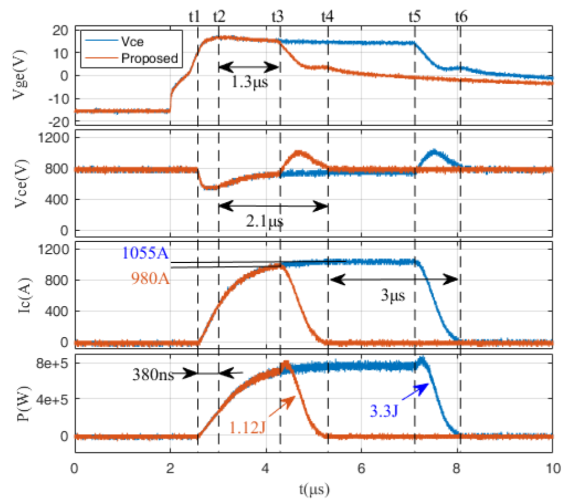

FIGURE 16. **Waveforms of short-circuit I test.**

time. According to IEC 60747-9 standard, the short-circuit withstand time (t_{psc}) of the proposed IPM is 2.06 μs. Compared to the V_{CE} desaturation detection method, the proposed method reduces the short-circuit energy loss, short-circuit peak current, fault duration, fault detection time and t_{psc} by 66%, 75 A, 3 μs, 4.12 μs and 57.7%, respectively.

In short-circuit II, the proposed method does not require the IPM to enter the short-circuit mode. When the current in the IPM exceeds the threshold, the module is turned off. In other words, to carry out fault detection and protective action, the proposed method does not wait for the I_C to rise to a very high value and desaturate the IGBT. The t_{psc} of the proposed method is only 0.62 μs. Compared to the V_{CE} desaturation detection method, the proposed method reduces the short-circuit loss, short-circuit peak current, fault duration, fault detection time and t_{psc} by 64.3%, 160 A, 1.6 μs, 3.1 μs and 61.5%, respectively.

The performance of the proposed IPM is compared with that of the conventional V_{CE} desaturation method in Table 4 . Different features of both methods shown in the table confirm

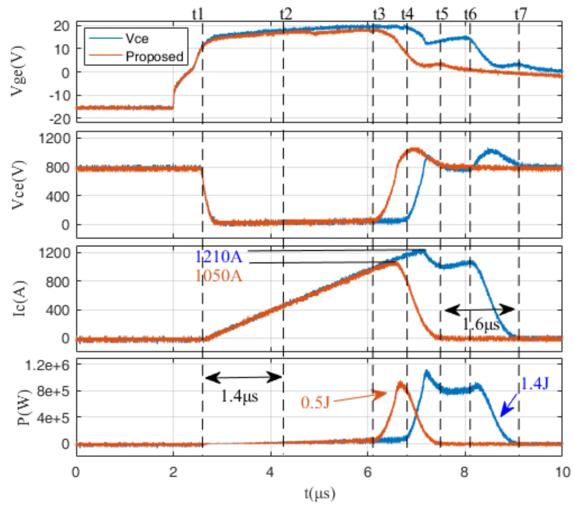

FIGURE 17. Waveforms of short-circuit II test.

TABLE 4. Comparison of conventional high-power ipm and proposed high-power ipm.

Features	Conventional IPM	Proposed IPM
I_c measurement method	Indirect	Direct
Does it have a blanking time?	Yes	No
Is the IGBT required to enter short-circuit mode during short-circuit II?	Yes	No
Time for detecting short-circuit I	1-5μs (4.5 μs in this paper)	Sub-microsecond (380 ns in this paper)
Time for detecting short-circuit II	1-5μs (4.5μs in this paper)	Less than 2μs (1.4μs in this paper)
Adaptability to different IGBT modules	Need to redesign blanking circuit	Based on triple rated current
Short-circuit energy loss	High	Low
Short-circuit withstand time	Long	Short
Fault duration	Long	Short

that the proposed high-power IPM is superior to the conventional V_{CE} desaturation method.

VIII. CONCLUSION

This paper presented a novel high-power IPM short-circuit protection design consisting of an internally integrated shunt, which directly measured I_C without any blanking time. The designed protection circuit could quickly detect all kinds of short-circuit faults. The feasibility of the proposed design for different types of short-circuits was verified via simulations and experiments, which showed that the shunt did not cause any heat dissipation and energy loss problems. The resistance of the shunt resistor did not change significantly for a switching frequency of less than 10 kHz. Fault-detection times of sub-microsecond level and less than 2 μs were achieved for short-circuit I and short-circuit II, respectively. The proposed high-power IPM design showed significantly improved performance compared to the conventional V_{CE} desaturation method. For short-circuit I, this improvement reduced the short-circuit energy loss, short-circuit peak current, fault duration, fault detection time and t_{psc} by 66%, 75 A, 3 μs, 4.12 μs and 57.7%, respectively. For short-circuit II, the short-circuit energy loss, short-circuit peak current, fault duration, fault detection time and t_{psc} were reduced by 64.3%, 160 A, 1.6 μs, 3.1 μs and 61.5%, respectively. In future work, we will optimize the IPM topology and layout while improving the protection circuit to decrease the response time.

REFERENCES

[1] A. Volke and M. Hornkamp, *IGBT Modules: Technologies, Driver and Application*, 2nd ed. Beijing, China: China Machine Press, 2016, pp. 60–74.

[2] M. Kudoh, Y. Hoshi, S. Momota, T. Fujihira, and K. Sakurai, "Current sensing IGBT for future intelligent power module," in *Proc. 8th Int. Symp. Power Semiconductor Devices ICs. (ISPSD)*, 1996, pp. 303–306.

[3] R. S. Chokhawala, J. Catt, and L. Kiraly, "A discussion on IGBT short-circuit behavior and fault protection schemes," *IEEE Trans. Ind. Appl.*, vol. 31, no. 2, pp. 256–263, Apr. 1995.

[4] B. Lu and S. K. Sharma, "A literature review of IGBT fault diagnostic and protection methods for power inverters," *IEEE Trans. Ind. Appl.*, vol. 45, no. 5, pp. 1770–1777, Nov. 2009.

[5] M. Khan and M. A. Rahman, "Development and implementation of a novel fault diagnostic and protection technique for IPM motor drives," *IEEE Trans. Ind. Electron.*, vol. 56, no. 1, pp. 85–92, Jan. 2009.

[6] L. Dulau, S. Pontarollo, A. Boimond, J.-F. Garnier, N. Giraudo, and O. Terrasse, "A new gate driver integrated circuit for IGBT devices with advanced protections," *IEEE Trans. Power Electron.*, vol. 21, no. 1, pp. 38–44, Jan. 2006.

[7] S. Musumeci, R. Pagano, A. Raciti, G. Belverde, C. Guastella, and M. Melito, "A novel protection technique devoted to the improvement of the short circuit ruggedness of IGBTs," in *Proc. 29th Annu. Conf. IEEE Ind. Electron. Soc. (IECON)*, Mar. 2003, pp. 1733–1738.

[8] L. Chen and F. Z. Peng, "Active fault protection for high power IGBTs," in *Proc. 24th Annu. IEEE Appl. Power Electron. Conf. Exposit.*, Feb. 2009, pp. 2050–2054.

[9] R. Pagano, Y. Chen, K. Smedley, S. Musumeci, and A. Raciti, "Short circuit analysis and protection of power module IGBTs," in *Proc. 20th Annu. IEEE Appl. Power Electron. Conf. Exposit. (APEC)*, May 2005, pp. 777–783.

[10] T. Krone, C. Xu, and A. Mertens, "Fast and easily implementable detection circuits for short circuits of power semiconductors," *IEEE Trans. Ind. Appl.*, vol. 53, no. 3, pp. 2715–2722, Jan. 2016.

[11] M. Takei, Y. Minoya, N. Kumagai, and K. Sakurai, "Analysis of IPM current oscillation under short circuit condition," in *Proc. 10th Int. Symp. Power Semiconductor Devices (ICs ISPSD)*, 1998, pp. 89–93.

[12] C. Kuratli, Q. Huang, and A. Biber, "Implementation of high peak-current IGBT gate drive circuits in VLSI compatible BiCMOS technology," *IEEE J. Solid-State Circuits*, vol. 31, no. 7, pp. 924–932, Jul. 1996.

[13] R. Graves, A. Lemmon, and L. Gant, "Fast, configurable over-current protection for high-power modules," in *Proc. IEEE Electr. Ship Technol. Symp. (ESTS)*, Jun. 2015, pp. 332–336.

[14] L. Pierre, B. Dominique, M. Herve, A. Bruno, and R. Jean-Francois, "Fast over-current protection of high power IGBT modules," in *Proc. Eur. Conf. Power Electron. Appl.*, 2005, pp. 1–10.

[15] Z. Wang, X. Shi, L. M. Tolbert, F. Wang, and B. J. Blalock, "A di/dt feedback-based active gate driver for smart switching and fast overcurrent protection of IGBT modules," *IEEE Trans. Power Electron.*, vol. 29, no. 7, pp. 3720–3732, Jul. 2014.

[16] Z. Wang, X. Shi, L. M. Tolbert, B. J. Blalock, and M. Chinthavali, "A fast overcurrent protection scheme for IGBT modules through dynamic fault current evaluation," in *Proc. 28th Annu. IEEE Appl. Power Electron. Conf. Exposit. (APEC)*, Mar. 2013, pp. 577–583.

[17] I. Ciocan, C. Farcas, D. Petreus, N. Palaghita, and A. Grama, "Over-current and short-circuit protection for IGBT's used in plasma generator inverter," in *Proc. IEEE 18th Int. Symp. Design Technol. Electron. Packag. (SIITME)*, Oct. 2012, pp. 341–345.

[18] F. Richardeau, P. Baudesson, and T. A. Meynard, "Failures-tolerance and remedial strategies of a PWM multicell inverter," *IEEE Trans. Power Electron.*, vol. 17, no. 6, pp. 905–912, Nov. 2002.

[19] F. Zhang, X. Yang, and Y. Ren, "Advanced active gate drive for switching performance improvement and overvoltage protection of high-power IGBTs," *IEEE Trans. Power Electron.*, vol. 33, no. 5, pp. 3802–3815, Jun. 2017.
[20] V. John, B.-S. Suh, and T. A. Lipo, "High-performance active gate drive for high-power IGBT's," *IEEE Trans. Ind. Appl.*, vol. 35, no. 5, pp. 1108–1117, Nov. 1999.
[21] Z. Dong, X. Wu, and K. Sheng, "Suppressing methods of parasitic capacitance caused interference in a SiC MOSFET integrated power module," *IEEE J. Emerg. Sel. Topics Power Electron.*, vol. 7, no. 2, pp. 745–752, Jun. 2019.
[22] S. Beczkowski, P. Ghimre, A. R. de Vega, S. Munk-Nielsen, B. Rannestad, and P. Thogersen, "Online Vce measurement method for wear-out monitoring of high power IGBT modules," in *Proc. 15th Eur. Conf. Power Electron. Appl. (EPE)*, Sep. 2013, pp. 1–7.
[23] P. J. Grbovic, "An IGBT gate driver for feed-forward control of turn-on losses and reverse recovery current," *IEEE Trans. Power Electron.*, vol. 23, no. 2, pp. 643–652, Mar. 2008.
[24] M. Chen, D. Xu, and X. Zhang, "An improved IGBT short-circuit protection method with self-adaptive blanking circuit based on V CE measurement," *IEEE Trans. Power Electron.*, vol. 33, no. 7, pp. 6126–6136, Jul. 2018.
[25] Y. Shi, R. Xie, L. Wang, Y. Shi, and H. Li, "Switching characterization and short-circuit protection of 1200 v SiC MOSFET T-type module in PV inverter application," *IEEE Trans. Ind. Electron.*, vol. 64, no. 11, pp. 9135–9143, Nov. 2017.
[26] M. A. Rodriguez-Blanco, A. Claudio-Sanchez, D. Theilliol, L. G. Vela-Valdes, P. Sibaja-Teran, L. Hernandez-Gonzalez, and J. Aguayo-Alquicira, "A failure-detection strategy for IGBT based on gate-voltage behavior applied to a motor drive system," *IEEE Trans. Ind. Electron.*, vol. 58, no. 5, pp. 1625–1633, May 2011.
[27] J.-B. Lee and D.-S. Hyun, "Gate voltage pattern analyze for short-circuit protection in IGBT inverters," in *Proc. IEEE Power Electron. Spec. Conf.*, Jul. 2007, pp. 1913–1917.
[28] M.-S. Kim, B.-G. Park, R.-Y. Kim, and D.-S. Hyun, "A novel fault detection circuit for short-circuit faults of IGBT," in *Proc. 26th Annu. IEEE Appl. Power Electron. Conf. Exposit. (APEC)*, Mar. 2011, pp. 359–363.
[29] K. Yuasa and S. I. Nakamichi Omura, "Ultra high speed short circuit protection for IGBT with gate charge sensing," in *Proc. IEEE 22nd Int. Symp. Power Semiconductor Devices IC's (ISPSD)*, Jun. 2010, pp. 37–40.
[30] F. Huang and F. Flett, "IGBT fault protection based on di/dt feedback control," in *Proc. IEEE Power Electron. Specialists Conf.*, Jul. 2007, pp. 1478–1484.
[31] L. Shu, J. Zhang, F. Peng, and Z. Chen, "Active current source IGBT gate drive with closed-loop di/dt and dv/dt control," *IEEE Trans. Power Electron.*, vol. 32, no. 5, pp. 3787–3796, May 2017.
[32] Y. Lobsiger and J. W. Kolar, "Closed-loop di/dt and dv/dt IGBT gate driver," *IEEE Trans. Power Electron.*, vol. 30, no. 6, pp. 3402–3417, Jun. 2015.
[33] K. Fink and S. Bernet, "Advanced gate drive unit with closed-loopdiC/dt control," *IEEE Trans. Power Electron.*, vol. 28, no. 5, pp. 2587–2595, May 2013.
[34] R. Hemmer, "Intelligent IGBT drivers with exceptional driving and protection features," in *Proc. 13th Eur. Conf. IEEE Power Electron. Appl. (EPE)*, Sep. 2009, pp. 1–4.
[35] E. R. Motto and J. F. Donlon, "IGBT module with user accessible on-chip current and temperature sensors," in *Proc. 27th Annu. IEEE Appl. Power Electron. Conf. Exposit. (APEC)*, Feb. 2012, pp. 176–181.
[36] M. Spang and N. Hofstoetter, "Evaluation of current measurement accuracy for a power module with integrated shunt resistors," in *Proc. Int. Exhib. Conf. Power Electron., Intell. Motion, Renew. Energy Energy Manage.*, May 2017, pp. 438–445.

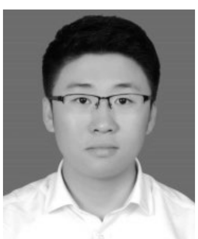

ZHAOLIANG MENG received the B.S. and M.S. degrees from the Xi'an University of Technology, Xi'an, China, in 2010 and 2013, respectively, where he is currently pursuing the Ph.D. degree in circuits and systems.

Since 2013, he has been working with Xi'an Polytechnic University. His research interest includes active gate drive and protection technologies of the high-power IGBTs.

YUAN YANG received the B.S., M.S., and Ph.D. degrees from the Xi'an University of Technology, Xi'an, China, in 1997, 2000, and 2004, respectively. From 2000 to 2004, she was a Lecturer, and an Assistant Professor, from 2004 to 2009. In 2005, she was a Visiting Scholar with Kyushu University, Japan. Since 2009, she has been working as a Professor with the Department of Electronics, Xi'an University of Technology. Her research interests include digital-analog mixed integrated circuit designs, the design of track circuit systems, gate drive and protection circuits of the high-power IGBTs, and wide-bandgap semiconductors.

YONG GAO received the B.S. degree in applied physics from the Xi'an University of Technology, Xi'an, China, in 1982, and the M.S. and Ph.D. degrees in microelectronics and solid-state electronics from Xi'an Jiaotong University, Xi'an, in 1988 and 1995, respectively. From 1996 to 2009, he was a Professor with the Department of Electronics, Xi'an University of Technology. Since 2010, he has been working as a Professor with the Department of Electronics, Xi'an University of Technology, and the Department of Electrical Engineering, Xi'an Polytechnic University, Xi'an. His research interests include power electronic devices, power integration and integrated circuit designs, and very large-scale integration designs.

SHENGSHENG AI was born in Shaanxi, China, in 1991. He received the B.S. degree from the Baoji University of Arts and Sciences, Baoji, China, in 2015. He is currently pursuing the M.S. degree with Xi'an Polytechnic University, Xi'an, China.

His research interest includes gate drive and protection technologies of SiC MOSFET IPM.

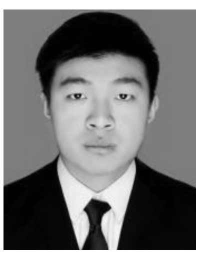

ZHENGPENG FANG was born in Henan, China, in 1993. He received the B.S. degree from the Henan University of Urban Construction, Pingdingshan, China, in 2018. He is currently pursuing the M.S. degree with Xi'an Polytechnic University, Xi'an, China.

His research interest includes wireless power transfer.

YANG WEN was born in Shaanxi, China, in 1990. He received the B.S. and M.S. degrees from Xi'an Polytechnic University, Xi'an, China, in 2012 and 2016, respectively. He is currently pursuing the Ph.D. degree in circuits and systems with the Xi'an University of Technology, Xi'an.

His research interest includes active gate drive and protection technologies of wide-bandgap semi-conductors.

LEI WU was born in Shaanxi, China, in 1984. He received the B.S. and M.S. degrees from the Xi'an University of Technology, Xi'an, China, in 2006 and 2011, respectively, where he is currently pursuing the Ph.D. degree in microelectronics and solid state electronics.

Since 2011, he has been working with CRRC Yongji Electric Company Ltd. His research interests include the reliability of high-power IGBTs.